Extremely Large Variations of Atmospheric ^{14}C Concentration During the Last Glacial Period

J. Warren Beck,[1]* David A. Richards,[2,3]* R. Lawrence Edwards,[3] Bernard W. Silverman,[4] Peter L. Smart,[2] Douglas J. Donahue,[1] Sofia Hererra-Osterheld,[1] George. S. Burr,[1] Leal Calsoyas,[1] A. J. Timothy Jull,[1] Dana Biddulph[1]

A long record of atmospheric ^{14}C concentration, from 45 to 11 thousand years ago (ka), was obtained from a stalagmite with thermal-ionization mass-spectrometric ^{230}Th and accelerator mass-spectrometric ^{14}C measurements. This record reveals highly elevated $\Delta^{14}C$ between 45 and 33 ka, portions of which may correlate with peaks in cosmogenic ^{36}Cl and ^{10}Be isotopes observed in polar ice cores. Superimposed on this broad peak of $\Delta^{14}C$ are several rapid excursions, the largest of which occurs between 44.3 and 43.3 ka. Between 26 and 11 ka, atmospheric $\Delta^{14}C$ decreased from ~700 to ~100 per mil, modulated by numerous minor excursions. Carbon cycle models suggest that the major features of this record cannot be produced with solar or terrestrial magnetic field modulation alone but also require substantial fluctuations in the carbon cycle.

A record of atmospheric radiocarbon variations to the measurement limit of ~50 ka is highly desirable as it is the basis for calibration of the ^{14}C time scale and it contains important information about variations in solar activity, Earth's magnetic field, the carbon cycle, and climate. In spite of nearly 50 years of effort, however, atmospheric radiocarbon variations before 16 ka remain poorly known. The most widely used records of ^{14}C variation for the Holocene and historical past (from 11.86 ka) are based on many continuous and overlapping tree-ring records (*1*). Before 11.86 ka, the record of atmospheric $\Delta^{14}C$ (*2*) is based principally on pointwise estimates with coupled ^{230}Th and ^{14}C ages of marine (*1*, *3–7*) and terrestrial carbonates (*8*), floating sequences of lacustrine or marine deposits (*9–13*), foraminifera from marine sediments cross calibrated with ice core records (*14*), or indirect records inferred from ^{10}Be or ^{36}Cl concentrations in polar ice cores or sediments (*15–18*). In general, these data become more sparse and scattered with increasing age. Records of past atmospheric ^{14}C concentration can also be generated with stalagmites (*19*), which are secondary calcite deposits formed by degassing of CO_2 from cave seepage waters. Here we present a high-resolution and nearly continuous record of ^{14}C variation derived from a stalagmite (GB-89-24-1) that was recovered from a submerged cave in the Bahamas (*20*) and dated with thermal-ionization mass-spectrometric (TIMS) ^{230}Th (*21*, *22*).

Calendar age (or ^{230}Th) chronology. Eighty-one TIMS U and Th analyses (*23*) were performed to obtain high-precision age estimates for subsamples distributed along the growth axis of the stalagmite (*24*) (Fig. 1). A small correction for initial ^{230}Th (i.e., unsupported by U) was made to each Th analysis on the basis of subsample ^{232}Th concentration and a calculated initial Th component with a $^{230}Th/^{232}Th$ activity ratio of 18.7 ± 2.9 ($2\sigma_m$; $n = 9$). Isochron techniques (*25*) were used to assess the initial $^{230}Th/^{232}Th$ ratio, which is at least an order of magnitude higher than the Bulk Earth value commonly used for initial Th corrections (*26*). For nearly all our samples, this correction was small because of low ^{232}Th concentrations, although the correction did reduce scatter (Fig. 1). The chronology generated with these techniques, which has also been verified with ^{231}Pa dating techniques (*27*, *28*), is remarkably coherent.

The relation between ^{230}Th age and longitudinal distance is smooth and nonlinear with a mean extension rate of ~19 mm ka^{-1}. We defined a distance–^{230}Th age relation to obtain a calendar age time scale because the stalagmite was sampled at different intervals for ^{230}Th and ^{14}C analyses (*29*). A weighted spline smoothing with a roughness penalty approach was used to achieve the best compromise between the residual error and curvature (*30*) for two growth phases separated by a hiatus from 28 to 26 ka, during which the drip locus moved a small distance laterally. A smoothing parameter based on the generalized cross validation method with the whole data set was applied to each of these two sections. Pointwise estimates of the 95% confidence intervals at each of the predictor values of distance were used to draw an error envelope about this spline function. For each of the ^{14}C subsample locations, we predicted the calendar age and 2σ error, which was based on interpolated functions of the upper and lower confidence interval bounds.

Radiocarbon measurements. Conventional ^{14}C measurements were made on 278 subsamples cut along the speleothem growth axis. We cut wafers, rather than milling or drilling powders, to minimize the risk of contamination by adsorbed atmospheric $^{14}CO_2$. Selective dissolution was undertaken for many samples to investigate the potential effects of secondary alteration (*31*). In all cases, there was no significant difference between the ^{14}C ages of successive dissolved fractions. Broken speleothem calcite, cemented into the base of GB-89-24-1, yielded a ^{230}Th age greater than 500 ka ($^{230}Th/^{238}U = 1.0015 \pm 0.0045$, $^{234}U/^{238}U = 1.0019 \pm 0.0037$) and was found to have a ^{14}C age >49.7 thousand years before present (ky B.P.), indistinguishable from that of the laboratory blank. This indicates that there was no postdepositional addition of ^{14}C while the speleothem was submerged in the cave.

Most stalagmites are secondary calcite deposits formed by degassing of CO_2 from cave seepage waters on exposure to cave atmosphere. The principal source of dissolved inorganic carbon in the seepage waters is soil CO_2 (derived from plant respiration and organic matter decay), which is effectively in equilibrium with the atmosphere at time scales greater than ~10 years. Generally, there is also a second component of carbon, the dead carbon fraction (DCF), which is derived from the host limestone surrounding the cave. This DCF is usually much older than 50 ka and thus contains negligible ^{14}C. The DCF introduces an age offset, which is analogous to a marine reservoir age correction (*32*, *33*) and must be subtracted from the radiocarbon age of the stalagmite material to reconstruct an atmospheric ^{14}C record.

To determine the DCF for GB-89-24-1, we compared the radiocarbon age versus calendar age relation with the widely used INTCAL98 compilation of calibration data (*1*) for the overlapping period of 11 to 16 ka. There is a reasonably constant ^{14}C age offset between the two sets of data (Fig. 2), which we attribute to DCF. The mean offset is 1450 ± 470 years (2σ; $n = 68$), which

[1]NSF-Arizona Accelerator Mass Spectrometry Facility, Department of Physics, University of Arizona, Tucson, AZ 85721, USA. [2]School of Geographical Sciences, University of Bristol, Bristol, BS8 1SS, UK. [3]Minnesota Isotope Laboratory, Department of Geology and Geophysics, University of Minnesota, Minneapolis, MN 55455, USA. [4]School of Mathematics, University of Bristol, Bristol, BS8 1TW, UK.

*To whom correspondence should be addressed. E-mail: wbeck@physics.arizona.edu, David.Richards@bristol.ac.uk

corresponds to a DCF of 16.5 ± 4.7% (2σ), similar to the range typically found for speleothems of 16 ± 5% (*34*, *35*). In spite of the strong resemblance between the GB-89-24-1 and INTCAL98 records suggesting nearly constant DCF, there are two moderate departures, which may be due to chronological errors in either GB-89-24-1 or INTCAL98 or, alternatively, to fluctuations in DCF. We are currently unable to resolve between these possibilities, although GB-89-24-1 is in better agreement with the Lake Suigetsu data (*13*) (Fig. 2) and the newly revised Cariaco Basin record (*12*), suggesting that revisions to INTCAL98 may be merited. Nevertheless, because of the uncertain origin of these two departures, we incorporate a conservative estimate of DCF uncertainty of 4.7% (2σ) in the overall precision of DCF-corrected ^{14}C age and $\Delta^{14}C$. This value is used, rather than $2\sigma_m$, because we acknowledge the possibility of residual structure in the ^{14}C age offset because of chronological differences, minor DCF variation, or differences in expected amplitude of variation between GB-89-24-1 and INTCAL98, which is based on the dampened signal of the mixed layer of the ocean. With this conservative error estimate, the relative contribution of uncertainty in DCF to the overall $\Delta^{14}C$ error diminishes with increasing calendar age from ~50% at 11 ka to ~10% at 45 ka.

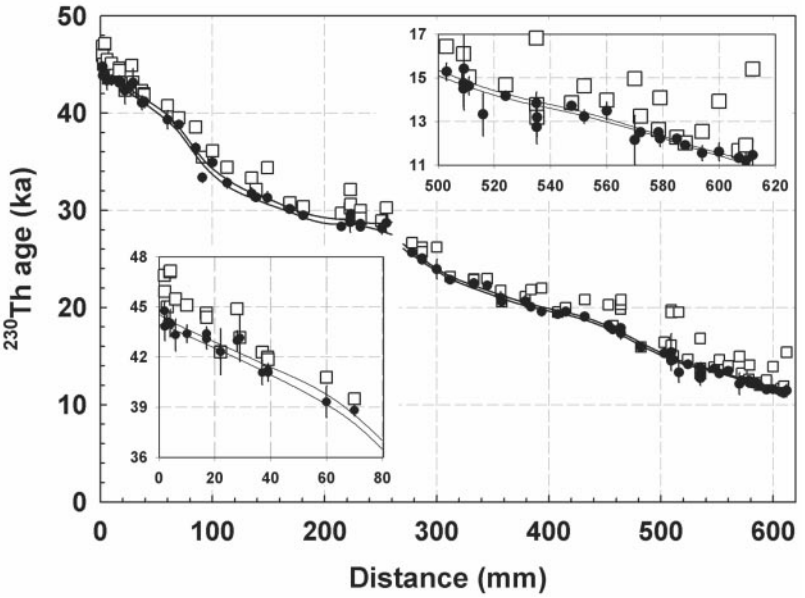

Fig. 1. ^{230}Th age versus distance along the longitudinal growth axis of GB-89-24-1, a submerged speleothem from –14.4 m in Sagittarius, Zodiac Caverns, Grand Bahama. ^{230}Th age is corrected for initial Th with $^{230}Th/^{232}Th_{init}$ activity ratio with a bulk Earth value of 0.8 ± 0.8 parts per million (□) and a substantially higher value of 18.7 ± 2.9 based on isochron results (●). The latter correction provides a smoother, monotonic distance-age relation. Confidence bands (95%) of a weighted smoothing spline with a roughness penalty approach (*30*) are plotted for each of the phases of growth before and after shift in drip locus between ~28 and 26 ka. These curves are used to predict calendar age and error for each of the subsamples selected for AMS ^{14}C analysis. Inset figures show expanded views of the oldest (bottom inset) and youngest (top inset) parts of the record.

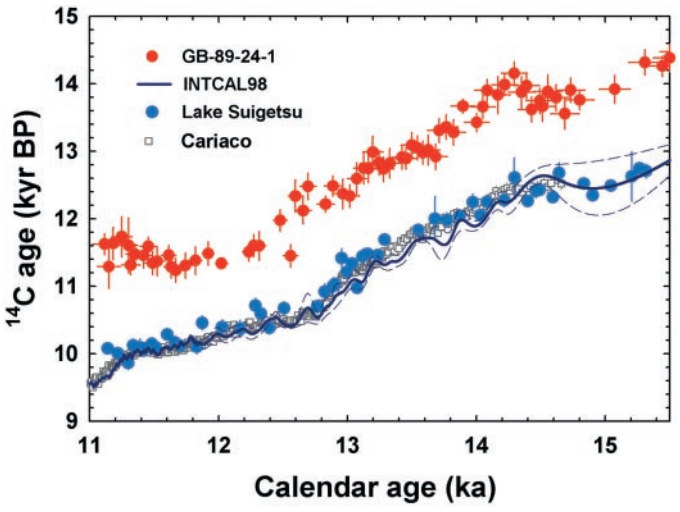

Fig. 2. Radiocarbon age versus calendar age for GB-89-24-1, Lake Suigetsu laminated sediments (*13*), and the INTCAL98 spline (*1*) for the period 15.5 to 11 ka. All ages are plotted with 2σ errors, except the INTCAL98 spline fit (1σ). Radiocarbon ages for GB-89-24-1 are not corrected for DCF; calendar ages and errors are based on the predicted longitudinal growth–^{230}Th age model with the spline fit illustrated in Fig. 1. Each set of data—speleothem, marine tree-ring compilation, and lake varves—shows a similar general pattern. The offset between INTCAL98 and GB-89-24-1 is relatively constant, with a mean value of 1450 ± 470 years (2σ) during a period of marked climate change. The constant offset is attributed to a relatively stable DCF of 16.5 ± 4.7 (2σ).

DCF-corrected ^{14}C ages for GB-89-24-1 show good agreement with other records between 11 and 26 ka (Fig. 3A), although before 30 ka, none of these records are in accord with each other. Between 30 and 45 ka, the Lake Suigetsu (*13*), Icelandic Sea (*14*), and Lake Lisan (*8*) records all exhibit generally older radiocarbon ages (or younger calendar ages) than GB-89-24-1. The Cango Cave record (*19*) is in general agreement with GB-89-24-1 although the data are sparse and its uncertainties are large. The available coral data (*4*, *7*) are in substantial agreement with GB-89-24-1 before 30 ka but reveal a high degree of scatter at older ages. One possible source of disagreement between GB-89-24-1 and other records between 30 and 45 ka could be fluctuations in DCF. We note, however, that large DCF fluctuations were not observed in GB-89-24-1 during the deglacial period, a period of marked climate change when DCF variability would be expected to be at a maximum. Furthermore, even if we were to allow DCF to go to its theoretical limit (i.e., no dead carbon), it still would not be possible to adjust GB-89-24-1 to match either the Icelandic Sea, Lake Suigetsu, or Lake Lisan records between 30 and 45 ka. We therefore assert that this discordance is largely due to other sources. Other possible sources of discordance between these records include incorrect initial ^{230}Th correction to ^{230}Th ages, unsupported gain or loss of U or Th, missing or uncounted varves in the Lake Suigetsu chronology, or, in the case of the Icelandic Sea record, uncertainty in the marine reservoir correction, errors in matching the ocean sediment $\delta^{18}O$ record to the Greenland Ice Sheet Project 2 (GISP2) $\delta^{18}O$ record, or uncertainties in the GISP2 chronology itself (*36*). We note parenthetically here that the Icelandic Sea record exhibits very similar structure to GB-89-24-1 and that an arbitrary 2-ka phase shift in calendar age before 25 ka brings these records into substantial agreement. This observation suggests that a discrepancy in calendar age may be the chief cause of disagreement between these two records.

The record of past atmospheric $\Delta^{14}C$ concentration derived from GB-89-24-1 (Fig. 3B) shows a broad maxima occurring between 44.5 and 33 ka, which can be divided

into a relatively short but intense excursion occurring between 44.3 and 43.3 ka and a much longer set of peaks between 42 and 33 ka B.P. The magnitude of the initial excursion is enormous, with the maximum values reaching ~1300 per mil (‰) (for the fitted spline), which is nearly twice as high as the "bomb-pulse" spike resulting from atmospheric nuclear weapons testing during the 1950s and 1960s. The other main features of this record are a marked drop in $\Delta^{14}C$ occurring between 35 and 33 ka, followed by a general 40% decline occurring between 26 and 11 ka. Smaller millennial-scale oscillations are superimposed on this latter decline, although some of these smaller oscillations may not be distinguishable from fluctuations caused by variations in DCF. Although it is possible that part of the largest excursions in $\Delta^{14}C$ excursion could be due to changes in DCF, we again note that even if DCF was reduced to the theoretical zero value, this 16.5% shift in DCF will only reduce these excursions by a small fraction. Thus, it is clear that the main cause of these large $\Delta^{14}C$ excursions is something other than fluctuations in DCF.

^{14}C modeling results. Enhancements in cosmogenic ^{36}Cl and ^{10}Be isotope concentrations at circa 30 to 45 ka have previously been observed in polar ice cores (*37*–*39*) and marine sediments (*40*), suggesting that atmospheric $\Delta^{14}C$ should also be elevated during this time frame. It has been known for some time that glacial age atmospheric ^{14}C levels were higher and more variable than during the Holocene (*16*, *17*, *41*), but the magnitude of variation revealed by our stalagmite record is nevertheless surprising. There are four main factors that can influence atmospheric ^{14}C concentration: primary cosmic ray flux, strength of the solar electromagnetic field, terrestrial magnetic field intensity, and the structure of the carbon cycle (*42*–*45*). The first three of these factors control the atmospheric ^{14}C production rate, whereas the fourth factor controls the distribution of ^{14}C between the various carbon reservoirs. Highly energetic galactic cosmic rays (GCR) account for most terrestrial ^{14}C production, although solar cosmic rays can account for a few percent of total production during brief periods of unusually energetic solar flare events (*42*, *46*). Although variation in GCR flux or energy spectra is one potential source of the observed variations in atmospheric $\Delta^{14}C$, it is generally thought to have remained fairly constant except on very long time scales ($>10^6$ years) (*46*). Electromagnetic fields associated with the Sun and solar wind and the terrestrial magnetic field intensity both modulate atmospheric ^{14}C production by attenuating the amount of GCR reaching Earth's atmosphere through a number of scattering mechanisms (*47*, *48*). These solar effects are modulated on the 11-year sunspot cycle (*49*, *50*) as well as several other longer cycles (*51*, *52*), which can produce about a factor of two variation in atmospheric ^{14}C production (*53*), with more production occurring during periods of low solar activity. For the normal range in cosmic ray energies incident on Earth's atmosphere, the globally integrated ^{14}C production rate also varies approximately in proportion to the inverse square root of Earth's magnetic field intensity [except at low geomagnetic field intensity where this relation diverges (*42*, *43*)]. At least a twofold variability in global ^{14}C production rate can be explained by the range of dipole magnetic field intensities during the past 50 ka (*42*, *43*).

To isolate which of these factors is responsible for the large observed variations in atmospheric $\Delta^{14}C$ for the period 45 to 11 ka, we performed several model simulations in which ^{14}C production regulation mechanisms were varied. For each simulation, a particular carbon cycle was specified because this substantially influences the distribution of ^{14}C between the various carbon reservoirs. We first chose the simplest case of an invariant balanced modern carbon cycle (*54*). Reservoir sizes and fluxes were brought to an initial balanced state in which both ^{12}C and

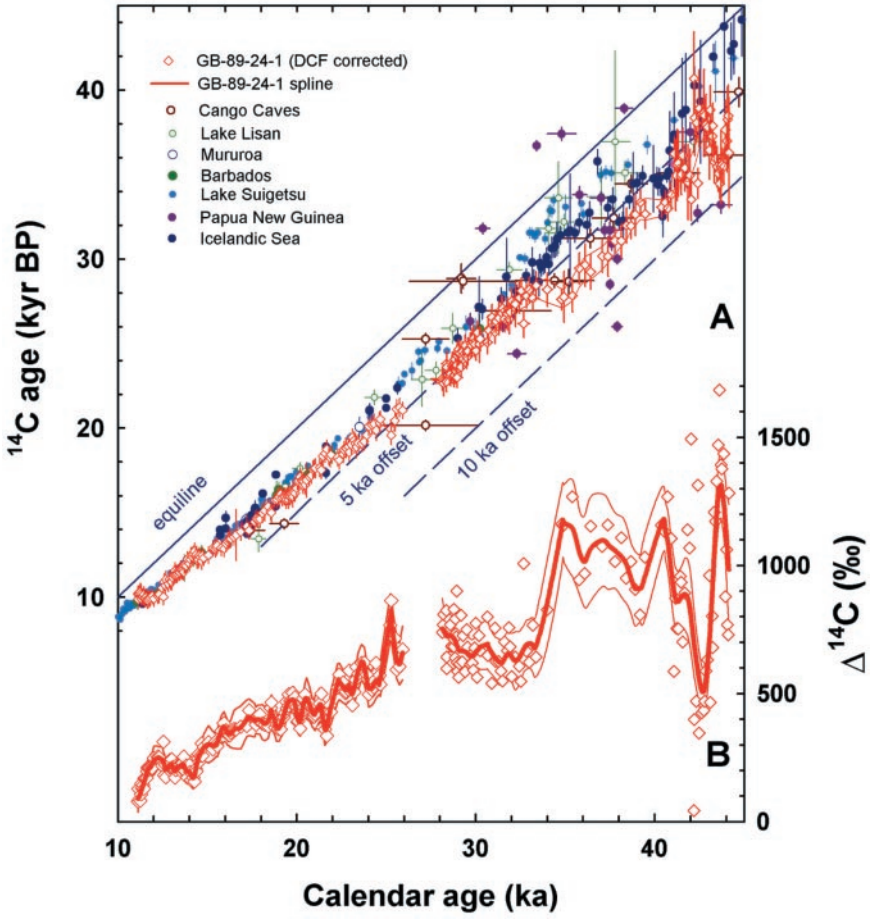

Fig. 3. Radiocarbon calibration curve and variations in atmospheric $\Delta^{14}C$ based on GB-89-24-1 from 45 to 11 ka and comparison with other $\Delta^{14}C$ records. (**A**) DCF-corrected ^{14}C age versus calendar age based on ^{230}Th ages for Bahamian stalagmite GB-89-24-1. Error bars for GB89-24-1 are 2σ and include uncertainty terms for ^{14}C measurement precision, ^{14}C chemical blank, DCF correction, and calendar age precision. Error bars are 2σ for all other data, except for Cango Caves (*19*), which are 1σ. This includes an uncertainty term for both ^{14}C measurement precision and calendar age precision, except for Icelandic Sea data (*14*), where zero uncertainty was assumed for calendar age precision. The Icelandic Sea foraminifera data are corrected with a marine reservoir age of 400 years. These records are fairly coherent back to ~32 ka but exhibit substantial scatter before this age. Prominent age reversals occur in the GB-89-24-1 ^{14}C time scale between 45 and 40 ka. (**B**) $\Delta^{14}C$ record for GB-89-24-1, including both raw data and smoothed spline with 95% confidence bands (thin red curves). A sharp peak of about 1 ka in duration is observed in GB-89-24-1 at circa 44 ka, reaching levels of about 1300‰—nearly twice as high as the 20th-century bomb pulse. Another broader $\Delta^{14}C$ maximum is observed between 42 and 33 ky B.P. This maxima appears to coincide broadly with the geomagnetic intensity minimum expressed in the SINT200 stacked geomagnetic record (*57*). Both peaks occur at about the same time as peaks of cosmogenic isotopes ^{10}Be and ^{36}Cl found in the Greenland Ice Sheet Project polar ice core (*38*, *39*).

^{14}C concentrations reflected the modern prebomb abundances (*45*, *55*, *56*). All model runs were initialized at 72 ka to eliminate any initial state transient behavior before entering the time window of interest (50 to 10 ka). In the first model run, we simulated the effects of geomagnetic modulation alone on ^{14}C production using the SINT-200 stacked paleomagnetic record (*57*). Results from this first model run matched the modern ^{14}C abundance for all carbon reservoirs after the 72-ka run time, and we obtained a long-term trend similar to that of Bard (*16*). This simulation, however, obtained peak levels of atmospheric Δ^{14}C that were about 700‰ lower than those observed in our stalagmite record for the magnetic field minima conditions between 40 and 35 ka and about 1000‰ lower than the peak values observed at the ~44-ka peak (Fig. 4A). In addition, the gradient of Δ^{14}C variations younger than 30 ka is much lower than that observed in GB-89-24-1 and other records. Thus, geomagnetic modulation alone cannot explain the variability in Δ^{14}C observed in GB-89-24-1. Simulation of a reduction of solar modulation to very low levels was also found to be insufficient to produce the GB-89-24-1 atmospheric Δ^{14}C record. Using the same carbon cycle model, and dropping solar electromagnetic modulation of GCR to zero for the length of the 44.3- to 43.3-ka excursion produces a Δ^{14}C excursion no greater than 150 to 200‰, which is only about one-fifth as large as required.

New paleomagnetic evidence from North Atlantic sediment cores (*58*, *59*) suggests that geomagnetic field intensity may have dropped to much lower strength during the Laschamp geomagnetic excursion than is represented by the SINT 200 record. During the Laschamp excursion, which apparently lasted about 1 ka on the basis of the duration of the inclination excursion, the magnetic field inclination may have rotated by as much as 180° with field intensity dropping to less than 10% of modern levels. The age of this excursion is controversial but is thought to be somewhere between 33 and 45 ka in age. Because the timing and duration of the Laschamp inclination excursion are similar to those of the ~44-ka ^{14}C excursion observed in our stalagmite record, it is plausible that the Laschamp excursion was coincident with this ^{14}C excursion. Nevertheless, our model simulations show that reducing both the solar and terrestrial magnetic fields to their theoretical limits of zero between 44.5 and 43.8 ka still produces only ~50% of the observed excursion amplitude and does not produce the high average levels of atmospheric Δ^{14}C observed in GB-89-24-1 (Fig. 4B). Thus, using a modern carbon cycle, we find that no combination of solar and geomagnetic modulation is capable of producing either the general trend or the large excursions observed in our atmospheric ^{14}C record. This implies that either the primary GCR flux has changed substantially during this time frame or that substantial changes in the carbon cycle must also have occurred during the past 50 ka, or both.

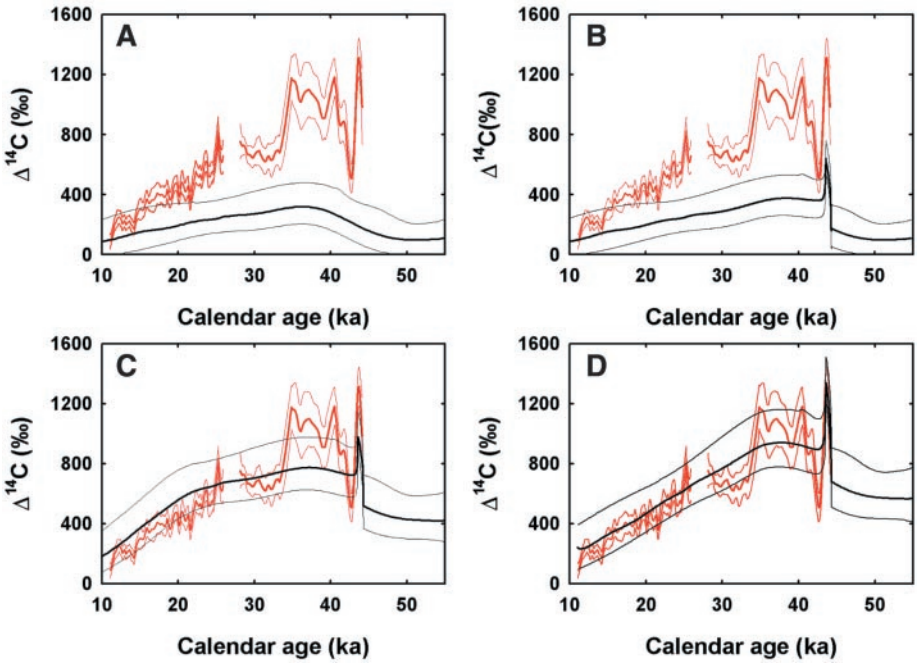

Fig. 4. Comparison between GB-89-24-1 Δ^{14}C, 45 to 11 ka (smoothing spline in red with 95% confidence intervals), and predicted atmospheric Δ^{14}C levels (black) from four 13-box carbon cycle model experiments (*54*). (**A**) Global ^{14}C production rate was modeled by varying geomagnetic field intensity only, with the SINT200 stacked-geomagnetic field record (mean and $\pm 1\sigma$) (*57*), and an invariant modern balanced carbon cycle with a steady state assumption was specified for this simulation (*54*). After 72 ka of run time, ^{14}C and ^{12}C levels returned to modern values in all model reservoirs. However, predicted atmospheric ^{14}C levels were substantially lower than observed in GB-89-24-1 during the last glacial period, and no major excursions were observed in the model output. (**B**) As in (A), except that both geomagnetic and solar magnetic fields were arbitrarily set to zero field strength between 44.5 and 43.8 ka. This experiment produced an atmospheric Δ^{14}C excursion of about 50% of the magnitude of the ~44-ka spike observed in GB-89-24-1 but failed to produce the generally high levels observed between 44 and 33 ka. (**C**) As in (B), except that the carbonate sedimentation rate was reduced to 0.24 Pg of C year^{-1} until 25 ka and then was gradually increased, reaching modern levels (2.0 Pg of C year^{-1}) at 11 ka. This model produced features similar to those observed in GB-89-24-1, but the ~44-ka excursion was smaller in amplitude than that observed in GB-89-24-1. (**D**) As in (C), except that the rate of thermohaline overturn was two-thirds of the modern level until 35 ka, when it was gradually increased, reaching modern levels at 11 ka. This model produced an even better match to the general features of the stalagmite record, and the ~44-ka excursion was of similar amplitude to that in GB-89-24-1. These models demonstrate that in addition to changes in ^{14}C production rate, changes in the carbon cycle are necessary to reproduce the GB-89-24-1 record of atmospheric ^{14}C.

Although the GCR flux is generally thought to have not varied substantially on time scales of $<10^6$ years (*46*), there is some evidence to the contrary. In particular, McHargue *et al.* (*40*) observe a very large ^{10}Be spike in sediments from the Gulf of California (circa 33 to 45 ka) with a peak ^{10}Be concentration that exceeds the theoretical limit predicted with the absence of both geomagnetic and solar modulation of GCR. They suggest that increased cosmic ray flux and other effects associated with a supernova shock wave transiting the solar system could have triggered both the geomagnetic field excursion and the large ^{10}Be anomaly observed synchronously in these sediments. Although this is a possible trigger for the ~44-ka Δ^{14}C excursion recorded in GB-89-24-1, we are unable to simulate the rapid decrease in atmospheric Δ^{14}C observed immediately after the ~1-ka excursion using a modern carbon cycle. This is because enhancement of ^{14}C production to this level for such a duration increases the ^{14}C concentration of the deep ocean reservoirs. These reservoirs have long residence times, and the return flux of ^{14}C from the ocean is sufficient to keep atmospheric Δ^{14}C elevated for an extended period. Thus, invoking an increase in GCR to explain the 44-ka spike would still seem to require the carbon cycle to have operated substantially differently than today.

We suggest that substantially different modes of the carbon cycle must be invoked to explain the high levels of atmospheric ^{14}C observed in our stalagmite record for the last

glacial period. Such high levels of atmospheric ^{14}C can be achieved by modulating carbonate sedimentation and dissolution rates or by changing the strength and/or depth of thermohaline circulation (THC). Both mechanisms result in increased storage of ^{14}C in the atmosphere when sedimentation rate is low or THC is sluggish or shallow. Figure 4C shows results from a model simulation identical to that presented in Fig. 4B, except that carbonate sedimentation rate was reduced to 0.24 Pg of C year^{-1} (*60*) until 25 ka and then gradually increased to modern levels (2.0 Pg of C year^{-1}) by the end of the last deglaciation (~11 ka). Equivalent and opposite changes in the dissolution flux from ancient (^{14}C depleted) sediments were also made to maintain a constant "active" carbon cycle size. This model simulation produces a first-order trend similar to the GB-89-24-1 record and exhibits increased sensitivity to rapid secular changes in geomagnetic field; however, it does not produce a ^{14}C excursion as large as that observed at ~44 ka even with the prescribed conditions of zero solar and terrestrial magnetic fields.

Modulating the strength and/or depth of THC can produce even larger atmospheric ^{14}C fluctuations than result from changing carbonate sedimentation rates. Figure 4D shows results of a model simulation identical to that shown in Fig. 4C, except that thermohaline circulation was also slowed to two-thirds (66%) of the modern level at the beginning of the model run and then progressively increased to modern levels (beginning at 35 ka and achieving modern levels by 11 ka). This simulation also produces a first-order trend similar to our stalagmite record and exhibits larger sensitivity to secular changes in geomagnetic field than produced by reducing the sediment rate alone.

In principle, all features of our stalagmite record could be produced with modulation of THC alone without having to invoke extreme conditions of solar and geomagnetic fields. To produce the largest ^{14}C excursion (~44 ka) observed in our stalagmite record would require a nearly stagnant ocean, however, in which thermohaline circulation was completely shut down. In one such scenario, placing a barrier to exchange at midthermocline depth in the ocean (~350 m) makes it possible to increase atmospheric $\Delta^{14}C$ at a rate of ~2‰ year^{-1} for the SINT200 geomagnetic conditions present at ~44 ka. A ^{14}C spike as large as the ~44-ka excursion can then be produced in the requisite period, and reconnection with deep ocean circulation would rapidly drop atmospheric ^{14}C to previous levels, as observed. The other excursions observed in our stalagmite record could also be produced in this manner. Although a stagnant ocean is certainly an extreme scenario, it is nevertheless interesting to speculate about possible breakdowns of THC as part of the explanation for the ^{14}C excursions because of the similar timing between the ~44-ka ^{14}C spike and Heinrich event H5 (*61*). Comparable but smaller ^{14}C excursions appear to occur in our record at roughly the same time as H4, H3, H2, and H1. Because Heinrich events may in some cases substantially reduce surface ocean salinity in the high-latitude oceans, a potential mechanism exists for modulating atmospheric $\Delta^{14}C$ by varying THC (*7*, *59*, *61*).

Extreme reduction of THC cannot, however, be invoked as a mechanism to produce the excursions in cosmogenic isotopes ^{10}Be and ^{36}Cl observed in sediments and ice cores between 30 and 45 ka (*37–39*, *62*). Excursions in the flux of these isotopes require substantially reduced solar or geomagnetic modulation of GCR or changes in primary GCR intensity. Because these ^{10}Be and ^{36}Cl excursions are due in part to the same phenomena that affect atmospheric ^{14}C, changes in the primary cosmic ray flux or the strength of the solar electromagnetic or geomagnetic field intensity must also contribute to our observed variations in atmospheric ^{14}C. Taken together, these ^{14}C, ^{10}Be, and ^{36}Cl records imply that both production rate changes and substantial fluctuations in the carbon cycle must be involved in producing the large observed fluctuations in atmospheric ^{14}C. Substantially slower or shallower thermohaline circulation and/or reduced carbonate sedimentation rates during the glacial are required to sufficiently enhance sensitivity to changes in production rate to match our record of atmospheric $\Delta^{14}C$. The cause of these implied changes in THC or carbonate sedimentation rates is unknown, but the observation that the carbon cycle apparently operated substantially more sluggishly in the recent past may have profound implications regarding the oceans' capacity to take up anthropogenic CO_2 emissions from fossil fuel burning.

References and Notes

1. M. Stuiver *et al.*, *Radiocarbon* **40**, 1041 (1998).
2. $\Delta^{14}C$ as used here is defined by the equation $\Delta^{14}C = 1000(Fe^{\lambda t} - 1)$ ‰, where F is the reservoir-corrected Fraction Modern, λ is the true ^{14}C decay constant, and t is the calendar age.
3. E. Bard *et al.*, *Nature* **382**, 241 (1996).
4. E. Bard, M. Arnold, B. Hamelin, N. Tisnerat-Laborde, G. Cabioch, *Radiocarbon* **40**, 1095 (1998).
5. G. S. Burr *et al.*, *Radiocarbon* **40**, 1093 (1998).
6. R. L. Edwards *et al.*, *Science* **260**, 962 (1993).
7. Y. Yokoyama, T. M. Esat, K. Lambeck, L. K. Fifield, *Radiocarbon* **42**, 383 (2000).
8. A. Schramm, M. Stein, S. L. Goldstein, *Earth Planet. Sci. Lett.* **175**, 27 (2000).
9. S. Björck *et al.*, *Science* **274**, 1155 (1996).
10. T. Goslar, M. Arnold, N. Tisnerat-Laborde, J. Czernik, K. Wiecedilckowski, *Nature* **403**, 877 (2000).
11. K. A. Hughen *et al.*, *Nature* **391**, 65 (1998).
12. K. A. Hughen, J. R. Southon, S. J. Lehman, J. T. Overpeck, *Science* **290**, 1951 (2000).
13. H. Kitagawa, J. van der Plicht, *Science* **279**, 1187 (1998).
14. A. H. L. Voelker *et al.*, *Radiocarbon* **40**, 517 (1998).
15. J. Beer, G. M. Raisbeck, F. Yiou, in *The Sun in Time*, C. P. Sonett, M. S. Giampapa, M. S. Matthews, Eds. (Univ. of Arizona Press, Tucson, AZ, 1991), pp. 343–359.
16. E. Bard, *Geochim. Cosmochim. Acta* **62**, 2035 (1998).
17. M. Frank, *Earth Planet. Sci. Lett.* **149**, 121 (1997).
18. R. Muscheler, J. Beer, G. Wagner, R. Finkel, *Nature* **408**, 567 (2000).
19. J. C. Vogel, J. Kronfeld, *Radiocarbon* **39**, 27 (1997).
20. GB-89-24-1, collected in 1989 from −14.4 m in Sagittarius, Zodiac Cavern 6, eastern Grand Bahama, is composed of dense, macrocrystalline calcite and shows no sign of postdepositional alteration. The longitudinal growth axis is 620 mm.
21. H. Cheng *et al.*, *Chem. Geol.* **169**, 17 (2000).
22. R. L. Edwards, J. H. Chen, G. J. Wasserburg, *Earth Planet Sci. Lett.* **80**, 241 (1987).
23. Of 81 U and Th measurements, 9 were duplicates split before chemical separation (either as powdered separates or chips from the same growth layer) and 5 were replicate dissolved and spiked samples put through chemistry separately.
24. Subsamples for ^{230}Th were drilled (<4-mm depth) at an angle oblique to the plane of the polished surface and parallel with growth layering. Time spans sampled for ^{230}Th analysis were intended to be similar to achievable age precision. Age estimates correspond to the midpoint along the longitudinal growth axis of each subsample.
25. K. R. Ludwig, D. M. Titterington, *Geochim. Cosmochim. Acta* **54**, 5031 (1994).
26. A. Kaufman [*Geochim. Cosmochim. Acta* **57**, 2303 (1993)] suggests using a worldwide $^{230}Th/^{232}Th$ activity value of 1.7 ± 0.7 in the absence of independent data.
27. R. L. Edwards, H. Cheng, M. T. Murrell, S. J. Goldstein, *Science* **276**, 782 (1997).
28. D. A. Pickett, M. T. Murrell, R. W. Williams, *Anal. Chem.* **66**, 1044 (1994).
29. Accelerator mass-spectrometric (AMS) ^{14}C analyses require a minimum of 1 mg of C (or 8.33 mg of $CaCO_3$) to obtain a 1σ precision of ~80 years at 12,000 yr B.P. and 1200 years at 40,000 yr B.P. Low U concentrations (59.1 to 228.1 ng g^{-1}) demanded calcite samples >0.5 g to obtain similar precision for ^{230}Th ages. Subsamples for ^{230}Th were drilled (<4 mm depth) at an angle oblique to the plane of the polished surface and parallel with growth layering. Time spans sampled for ^{230}Th analysis were intended to be similar to achievable age precision. Age estimates correspond to the midpoint along the longitudinal growth axis of each subsample.
30. P. J. Green, B. J. Silverman, *Nonparametric Regression and Generalized Linear Models* (Chapman & Hall, London, 1994).
31. G. W. Burr, R. L. Edwards, D. J. Donahue, E. R. M. Druffel, F. W. Taylor, *Radiocarbon* **34**, 611 (1992).
32. E. Bard, *Paleoceanography* **3**, 635 (1988).
33. E. Bard *et al.*, *Earth Planet Sci. Lett.* **126**, 275 (1994).
34. D. Genty, M. Massault, *Radiocarbon* **39**, 33 (1997).
35. D. Genty *et al.*, *Radiocarbon* **41**, 251 (1999).
36. R. B. Alley *et al.*, *J. Geophys. Res.* **102**, 26367 (1997).
37. G. M. Raisbeck *et al.*, *Nature* **292**, 825 (1981).
38. S. Baumgartner *et al.*, *Science* **279**, 1330 (1998).
39. F. Yiou *et al.*, *J. Geophys. Res.* **102**, 26783 (1997).
40. L. R. McHargue, P. Damon, D. J. Donahue, *Geophys. Res. Lett.* **22**, 659 (1995).
41. E. Bard, B. Hamelin, R. Fairbanks, A. Zindler, *Nature* **345**, 405 (1990).
42. J. Masarik, J. Beer, *J. Geophys. Res.* **104**, 12,099 (1999).
43. D. Lal, in *Solar-Terrestrial Relationships*, G. C. Castagnoli, D. Lal, Eds. (Soc. Italiana di Fisica-Bologna-Itala, Bologna, Italy, 1988), pp. 216–233.
44. _____, B. Peters, in *Progress in Elementary Particle and Cosmic Ray Physics*, J. G. Wilson, S. A. Wouthuysen, Eds. (North-Holland, Amsterdam, 1962), pp. 1–74.
45. E. T. Sundquist, W. S. Broecker, Eds., *The Carbon Cycle and Atmospheric CO_2: Natural Variations Archean to Present*, vol. 32 of Geophysical Monograph Series (American Geophysical Union, Washington, DC, 1985).
46. R. Reedy, in *Solar Particle Events and Their Radiation Threats, Conference on the High Energy Radiation Background in Space, Snowmass, CO* (IEEE Nuclear

and Plasma Sciences Society and the Institute of Electrical and Electronic Engineers, location, 1998), pp. 317–323.
47. E. N. Parker, in *Cosmic Winds and the Heliosphere*, J. R. Jokipii, C. P. Sonett, M. S. Giampapa, Eds. (Univ. of Arizona Press, Tucson, AZ, 1997), pp. 3–27.
48. E. J. Smith, in *The Sun in Time*, C. P. Sonett, M. S. Giampapa, M. S. Matthews, Eds. (Univ. of Arizona Press, Tucson, AZ, 1991), pp. 175–201.
49. P. Damon, C. P. Sonnet, in *The Sun in Time*, C. P. Sonnet, M. S. Giampapa, M. S. Matthews, Eds. (Univ. of Arizona Press, Tucson, AZ, 1991), pp. 360–388.
50. M. Stuiver, *J. Geophys. Res.* **66**, 273 (1961).
51. J. C. Houtermans, thesis, University of Bern, Bern, Switzerland (1971).
52. H. E. Suess, *Radiocarbon* **22**, 200 (1980).
53. K. O'Brien, A. D. L. Z. Lerner, M. A. Shea, D. F. Smart, in *The Sun in Time*, C. P. Sonnet, M. S. Giampapa, M. S. Matthews, Eds. (Univ. of Arizona Press, Tucson, AZ, 1991), pp. 317–343.
54. A 13-box carbon cycle model was used that included reservoirs for the atmosphere, terrestrial biosphere, soils, ocean sediments, and a 9-box ocean. Reservoir size and fluxes were brought to an initial balanced state in which both ^{12}C and ^{14}C concentrations reflected the modern prebomb pulse abundances (*45*, *55*, *56*). A globally averaged modern ^{14}C production rate of 2.03 atoms cm^{-2} s^{-1} was used (*42*), although this value is probably uncertain to about ±10% (*63*). The terrestrial magnetic field intensity dependence used (*42*) assumes a solar modulation parameter of ϕ = 550 equal to an average value for the period 1953–95, whereas the SINT200 (*57*) stacked paleomagnetic record was used as the record of terrestrial magnetic field intensity. The total active carbon reservoir size was set at 54,600 Pg of C, as required by a steady state ^{14}C production rate of 2.03 atoms cm^{-2} s^{-1} and the known modern ^{14}C activities in the various reservoirs (*55*). We define the active carbon reservoir as that carbon that may exchange with the atmosphere on 50-ka time scales. Because the production rate could only have been greater in the past 50 ka (because we are now at a geomagnetic maximum), the minimum size of the active carbon cycle is determined in the following way: If $(\partial N/\partial t)$ global = 2.03 atoms cm^{-2} s^{-1} × area of Earth, then the global ^{14}C inventory is given by $(\partial N/\partial t)$ global/λ_{14C} (global), and the inventory of ^{12}C is given by ^{14}C(global)/($^{14}C/^{12}C$)average = ^{12}C(active carbon cycle). Thus, ^{12}C(active carbon cycle) = 54,600 Pg of C. Because there are only 39,400 Pg of C (*45*) in the ocean + atmosphere + biosphere + active terrestrial soils, this means there are additionally about 15,200 Pg of C contained in other parts of the active carbon cycle. The only element of the active carbon cycle large enough to contain this amount of carbon is ocean carbonate sediments. If these sediments are formed in the ocean mixed layer, then the initial ($^{14}C/^{12}C$) must be the same as that of the mixed layer (i.e., FM = 0.85). This implies that at steady state the flux of carbon to this sedimentary sink must be on average 1.85 Pg of C $year^{-1}$.
55. W. S. Broecker, T.-H. Peng, *Tracers in the Sea* (Lamont-Doherty Geological Observatory, Palisades, NY, 1982).
56. G. Munhoven, thesis, Université de Liége, Liége, Belgium (1997).
57. Y. Guyodo, J.-P. Valet, *Earth Planet. Sci. Lett.* **143**, 23 (1996).
58. C. Laj, C. Kissel, A. Mazaud, J. E. T. Channel, J. Beer, *Philos. Trans. R. Soc. London* **358**, 1009 (2000).
59. C. Kissel *et al.*, *Earth Planet. Sci. Lett.* **171**, 489 (1999).
60. Most estimates of carbonate sedimentation rates for the modern world range between 0.24 and 2.0 Pg of C $year^{-1}$.
61. H. Heinrich, *Quat. Res.* **29**, 143 (1988).
62. P. E. Damon, R. E. Sternberg, *Radiocarbon* **31**, 697 (1989).
63. R. C. Finkel, K. Nishiizumi, *J. Geophys. Res.* **102**, 26699 (1997).
64. This paper is dedicated to the memory of R. Palmer and R. Parker, who died in separate diving incidents in 1997. We are extremely grateful to both of them for their invaluable contributions to exploration and fieldwork in the Blue Holes of the Bahamas.

17 October 2000; accepted 24 April 2001
Published online 11 May 2001;
10.1126/science.1056649
Include this information when citing this paper.

REPORTS

Ultrafast Manipulation of Electron Spin Coherence

J. A. Gupta,[1] R. Knobel,[2] N. Samarth,[2] D. D. Awschalom[1]*

A technique is developed with the potential for coherent all-optical control over electron spins in semiconductors on femtosecond time scales. The experiments show that optical "tipping" pulses can enact substantial rotations of electron spins through a mechanism dependent on the optical Stark effect. These rotations were measured as changes in the amplitude of spin precession after optical excitation in a transverse magnetic field and approach $\pi/2$ radians. A prototype sequence of two tipping pulses indicates that the rotation is reversible, a result that establishes the coherent nature of the tipping process.

Multiple pulse sequences in time-domain nuclear magnetic resonance and electron spin resonance (ESR) experiments are widely used to study spin-spin interactions and spin dephasing in inhomogeneous magnetic environments (*1*). A canonical sequence consists of a $\pi/2$ pulse to generate a nonequilibrium transverse spin polarization followed by a π-pulse that may enact a rephasing ("spin echo") of transverse spin if inhomogeneous broadening dominates the ensemble spin dynamics (*2*). Current technology limits the number of systems to which pulsed-ESR experiments can be applied because the minimum achievable pulse length of ~10 ns should be much smaller than the spin coherence time (*1*). To apply pulse sequences to study conduction-band electron spin dynamics in a variety of semiconductors where spin lifetimes can vary from ~3 ps (*3*) to ~130 ns (*4*), a complementary ESR technique capable of much shorter pulse widths is desirable. Application of spin echo sequences might be of particular interest in semiconductor quantum dots, where inhomogeneous broadening can limit spin lifetimes (*5*). Such a technique could also be useful for spin-based implementations of quantum computing in solid-state systems (*6*), where it is necessary to perform many operations ($>10^4$) on a quantum bit within the coherence time to realize full computation with error correction (*7*). The ability to perform spin operations on femtosecond time scales would satisfy this need in a number of semiconductor systems and may be applicable to single quantum bits using optical probes with high spatial resolution.

Here we present time-resolved Faraday rotation experiments that extend a technique first applied in atomic sodium (*8*) to semiconductor nanostructures by using ultrafast laser pulses to produce coherent rotations of electron spins (*9*). In our experiments, a pump pulse optically excites spin-polarized electrons that precess about a static magnetic field. A second below–band gap "tipping" pulse produces an additional effective magnetic field that can reach 20 T through the optical Stark effect (*10*). Effective field strengths are calculated from measurements of Stark shifts and depend on the pulse intensity, polarization, and energy. This field is used to coherently rotate electron spins by angles that approach $\pi/2$, as monitored through the Faraday rotation imparted to a probe pulse. A sequence of two tipping pulses suggests that spin coherence is preserved during the tipping process. Because the tipping pulses additionally excite a small number of real carriers, a variety of checks were performed to identify resultant background contributions. Although the tipping effects can be qualitatively interpreted as rotations about a light-induced effective field, quantitative comparisons of the tipping angle from Faraday rotation data with that expected from measured Stark shifts reveal a significant discrepancy.

Samples were chosen that illustrate a variety

[1]Department of Physics, University of California, Santa Barbara, CA 93106, USA. [2]Department of Physics, The Pennsylvania State University, University Park, PA 16802, USA.

*To whom correspondence should be addressed. E-mail: awsch@physics.ucsb.edu